Arab J. Nucl. Sci. Appl., Vol. 54, 1, 85-96 (2021)

Arab Journal of Nuclear Sciences and Applications

ISSN 1110-0451 ***Web site: ajnsa.journals.ekb.eg*** **(ESNSA)**

Viscoplastic Creep Characterization of Novel Sn–0.7Cu-0.2Ni–xAl Lead-Free Solders for Electronic Applications

Mahmoud S. Dawood[a], S. A. Eladly[b], A. M. El-Taher[a]
[(a)] *Physics Department, Faculty of Science, Zagazig University, Zagazig, Egypt*
[(b)] *Modern Academy of Engineering and Technology, Basic Sciences Department, Cairo, Egypt*

Received 20th Jan. 2020
Accepted 20th Feb. 2020

The effects of adding 0.1-0.2wt%Al on microstructure and creep properties of Sn–0.7Cu-0.2Ni (SCN) alloys were investigated. The presence of Ni in SCN alloy inhibits the polymorphic transition of Cu_6Sn_5 IMC particles and forms a more stable (Cu,Ni)6Sn5 IMC particles. After Al-microalloying, the Sn–0.7Cu-0.2Ni–xAl alloys exhibit a heterogeneous structure with an additional fine Al_3Ni_2 and Al_2Cu IMC phases and coarse $(Cu,Ni)_6Sn_5$ IMCs. Adding 0.1%Al to SCN solder is the most effective in softening while the creep rate and yield strength is slightly maintained down to the SCN solder level. Hence, the desirable creep property attained in SCN-0.1 wt%Al solder could play a significant role in the improvement of drop impact performance in electronic devices. The creep deformation at stresses of 8.8–23.4 MPa is characterized by stress exponents of 4.4-5.0 and activation energy of 46.8-53.9 kJ.mol^{-1} close to that for pipe-diffusion of Sn, which are typical of dislocation creep mechanism.

Keywords: *Lead-Free Solders, Sn-Cu Alloys, Viscoplastic Creep*

Introduction

Considering the current electronic industry trend for creating high-performance structural materials, lead-free Sn-Cu solders become one of the most candidate alloys for various electronic applications, especially for wave soldering, dip and iron soldering at high temperature applications [1]. The major action taken to achieve the integrity of Sn-Cu alloys and develop their elastic compliance is to ensure their mechanical reliability, which requires solder joints with large ductility and high strength [2, 3]. More specifically, even though the insufficient mechanical strength, solidus polymorphic transformation of Cu_6Sn_5 phase and lower ductility of Sn-Cu alloys are trade-off material properties, the development of microstructure could result in an improvement of the entire properties. This, in turn, further emphasizes the importance of understanding creep mechanisms of Sn-Cu solders and their corresponding microstructure evolution, which could predict the structural performance of these solders and evaluating the associated final mechanical reliability [4].

The polymorphic transition of Cu_6Sn_5 phase is acknowledged to be one of the main challenges that must be overcome to improve the reliability of Sn-Cu solders. In accordance with the Sn–Cu phase diagram, the eutectic composition of Sn–0.7wt.%Cu alloy includes Cu_6Sn_5 IMC and β-Sn as a principal phase at 25°C [5]. During cooling the Sn–0.7wt.%Cu alloy molten, the polymorphic hexagonal η-Cu_6Sn_5 phase, formed at a higher temperature of 227°C, is converted into monoclinic ή-Cu_6Sn_5 phase at a lower temperature of 186°C without compositional variation [6]. This solidus polymorphic transition of Cu_6Sn_5 phase is believed to be one of the adverse issues affecting the reliability of SC solder joints. To alleviate these trepidations, the tempting strategy here is to adapt the composite route of hard and soft alloy phases which improves the solder reliability. Generally

Corresponding author: mah_sol@hotmail.com
DOI: 10.21608/ajnsa.2021.29270.1349

creep is a complicated metal deformation route. This time-dependent deformation behavior takes place at high temperatures and stresses. Information about the impact of the second phase formation on the creep deformation of the Sn-Cu alloys is important for assessing their reliability and design.

Studies analyzing the influence of microalloying elements on the stability of hexagonal η-Cu_6Sn_5 phase have been reported. For instance, doping of microalloying of Ni in SC solder was found to obstruct the polymorphic transformation owing to the formation of hexagonal $(Cu,Ni)_6Sn_5$ IMC, which is not only thermodynamic stable at 25°C, but also will prevent the volume change linked with phase transition and inhibit IMC cracking [7, 8]. Ni has enhanced the corrosion resistance of SC solders [9, 10]. Thus , several studies also have been reported on alloying of Zn, In, Au and Sb to stabilize the hexagonal η-Cu_6Sn_5 phase [11-13]. Moreover, a growing attention has been paid to Sn–Cu–Ni (SCN) and Sn–Ag–Cu (SAC) alloys containing rare earth (RE) elements including Ce, Nd and Pr to enhance their performances. Survey of the current literature [14-17] showed a significant decrease in grain size of SAC and SCN solders with microalloying of REs. However, due to the high cost of REs, Al element is acknowledged as a cheap material and non-harmful because of its plentiful availability. The modifications of the SC alloy system by Al microalloying exhibited outstanding. More specially, refinement of IMCs and mechanical performances [18]. In spite of the forceful effect of Al on solderability of SC solders, the assigned mechanism is not entirely understood. Even through, the operative results are reasonable for SC solders in most cases, knowledge about the newly Sn-0.7Cu-0.2Ni solder alloy system is very limited especially regarding the influence of microalloying of Al.

The aim of present study is understanding the creep mechanisms responsible for enhancing the coexisting trade-off between creep resistance and ductility in the SCN alloy. Therefore, creating heterogeneous-structure depending on Al content is proposed. The addition of Al is believed to enhance gaining fine-scaled eutectic microstructures that enables improving the creep resistance, which is generally associated with heterogeneous structure that improves the ductility in the SCN alloy. Consequently, the bulk microstructure and tensile creep behaviors of a series of Pb-free SCN-xAl alloys were examined and discussed in this study.

Experimental Procedures

The Sn-0.7Cu-0.2Ni (SCN) master alloy is nominally composed of (by weight percent) 99.1% Sn, 0.7% Cu and 0.2% Ni elements. The pure elements (4N purity) of the master alloy with Al contents of 0,1 and 0.2 wt% are prepared and remelted three times at 700°C for 60min to endorse their homogeneity. The produced SCN-xAl alloys; SCN, SCN-0.1wt.% Al and SCN-0.2 wt.%Al alloys are allowed to cool at air cooling conditions. The cast bars of the three alloys were cold drawn into cylindrical-shaped of wire samples of 4×10^{-2} m length and 2.5mm diameter [19]. All specimens were subsequently homogenized at 120°C for 60 min in electric furnace before being endorsed to cool at room temperature. The condition of annealing was resolved after performing several tests with different temperature and time that permits the residual stress to be moderately removed. The chemical compositions explored by x-ray fluorescence (XRF) are listed in Table (1). The microstructural analysis of the three alloys was yielded by neatly polished using 0.5μm Al_2O_3 particles and chemically etched in 6% solution of 3%HCl and 3%HNO_3 with 94 % ethyl alcohol for few seconds. The etchant solder was then conducted with a scanning electron microscope (SEM) [Philips XL-30 model, Japan] to explore the microstructure. The energy dispersive spectroscopy (EDS) was utilized to inspect the phase compositions with mapping of their distributions. Also, the initially-cold-drown and processing samples were assessed using X-ray diffractometer (XRD) [Philips Analytical X-Ray PW3710] with Cu Kα radiation at 40kV and 20 MA at angles range of 10 - 90° with a scanning rate of 6°C min^{-1}. To claim the impacts of added Al microalloying and thermo-mechanical processing on the mechanical behavior of SCN solder, tensile creep tests were performed using a standard testing machine [20], at a temperature range 25-110 °C and applied a stress range of 8.8 – 23.4 MPa. To explore the impacts of Al microalloying on the strength and ductility of three solders, tensile stress-strain tests were performed at room temperature for the SCN, SCN-0.1wt.% Al and the SCN-0.2 wt.%Al alloys.

Table (1): Chemical composition of the three solders studied (wt.%)

Alloy	Cu	Ni	Fe	As	Pb	Al	In	Sn
Sn-0.7Cu-0.2Ni	0.707	0.201	0.003	0.002	0.002	0.00	0.002	Bal
Sn-0.7Cu-0.2Ni-0.1Al	0.703	0.203	0.003	0.002	0.003	0.102	0.002	Bal
Sn-0.7Cu-0.2Ni-0.2Al	0.705	0.202	0.003	0.002	0.003	0.204	0.002	Bal

Experimental Results and Discussion

Phase analysis of SCN-xAl alloys

To address the determination of main phases formed in various alloy compositions, XRD analysis was performed and results are shown in Fig.(1). The anticipated lines from the eutectic phases; β-Sn, Cu_6Sn_5 and $(Cu,Ni)_6Sn_5$, are recognized and no further phases were established in plain SCN alloy, in agreement with microstructure presented in Fig. (2). However, most of Cu_6Sn_5 IMCs are transformed into $(Cu,Ni)_6Sn_5$ IMC owing to the presence of Ni in the SCN alloy[21]. The appearance of the thermodynamic stable IMCs such as $(Cu,Ni)_6Sn_5$ particles inside the melt is supposed to be the foremost prerequisite for heterogeneous nucleation. Microalloying of Al assists creation of additional fine particles of Al_2Cu and Al_3Ni_2 IMCs, which appeared as small peaks in XRD and established from EDS analysis. It is evident that Al-microalloying has successfully shrunk the peak intensity of β-Sn phase at 2θ = 31.6° and 63.5°, while amplified the peak intensity of $(Cu,Ni)_6Sn_5$ IMCs. This specifies that the grain size of β-Sn is refined, while that of $(Cu, Ni)_6Sn_5$ IMCs is coarsened after Al additions. Hence, the coupling effect resulted in grain size modification and heterogeneity of dislocation density after Al-microalloying is predictable, causing extensively scattered values of strength through different length scales of the solder matrix.

Morphologies of SCN-xAl alloys

The microstructures of the examined SCN alloy employing equiaxed β-Sn grains and eutectic precipitates with irregular polygons of Cu_6Sn_5 and $(Cu,Ni)_6Sn_5$ IMC are shown in SEM micrographs in Fig.(2). It is interesting to note that the presence of 0.2 wt% Ni element in the SCN solder leads to the formation of a large number of small $(Cu, Ni)_6Sn_5$ particles on account of the high affinity of Ni to Cu element. This declaration is consensus with that reported by Ramli et al. [22], where the microalloying of the Ni in Sn-0.7Cu solder resulted in diminishing the growth of $(Cu,Ni)_6Sn_5$ IMCs.

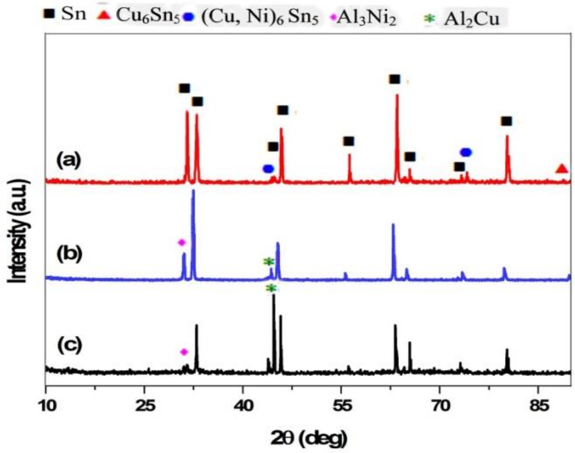

Fig. (1): XRD pattern for SCN, SCN-0.1%Al and SCN-0.2%Al solder alloys

Al was acknowledged to inspire the growth of $(Cu, Ni)_6Sn_5$ IMCs in SCN-*x*Al solder alloys. The morphology and size of IMCs particles were found to depend on the Al content. As seen in Fig.(2b), the size and morphology of $(Cu,Ni)_6Sn_5$ IMCs were noticeably increased after 0.1% Al-microalloying. The needle-like $(Cu,Ni)_6Sn_5$ IMCs are formed while some fairly fine dot particles of Al_2Cu and Al_3Ni_2 are created at the expense of the Cu and Ni contents. Although the plain SCN solder comprises the entirely homogeneous structure involving fine eutectic particles, the SCN-xAl alloys are characterized by heterogeneous structure with a combination of both fine Cu_6Sn_5, Al_2Cu and Al_3Ni_2 particles (length of ~5-10 µm) and coarser $(Cu, Ni)_6Sn_5$ particles (length of ~25-60 µm). Hence, the coupling effect resulted in grain size modification and heterogeneity of dislocation density after Al-microalloying is predictable, causing extensively scattered values of strength through different length scales of solder matrix. The substantial effect of this heterogeneous structure is the accomplishment of a unique combination of creep resistance and large ductility in the Al-containing specimens as can be seen later. One can expect that the heterogeneous structures could result in strain hardening mechanism that could stabilize the microstructure and create high ductility. This mechanism is

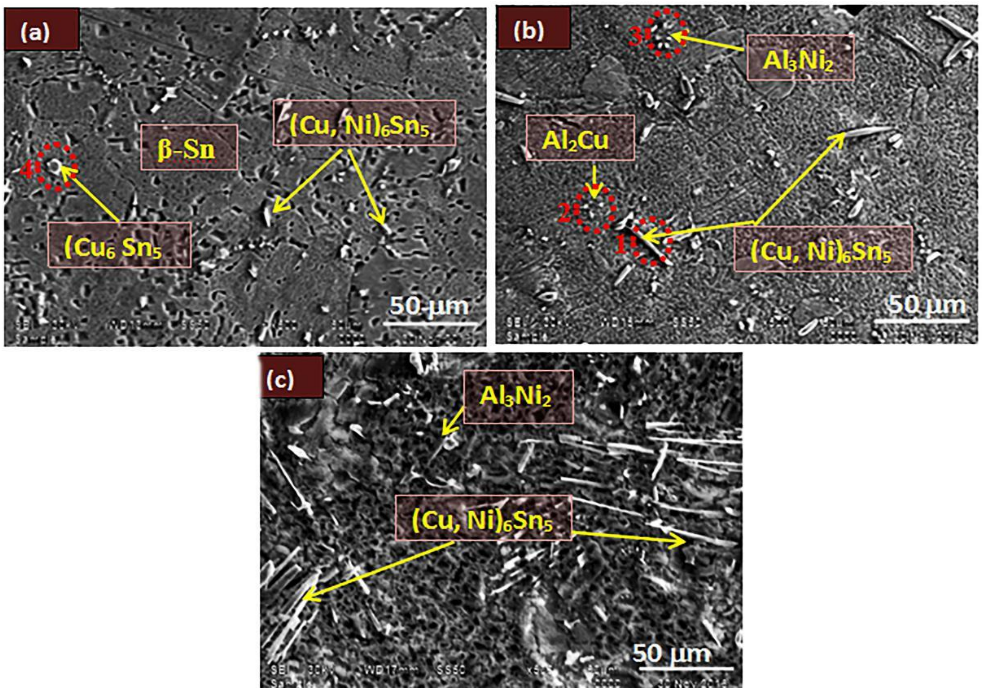

Fig. (2): The SEM micrographs of (a) (SCN), (b) (SCN-0.1Al) and (c) (SCN-0.2Al) alloys

extensively clarified and discussed in literature [23-25]. As a result, the potential of the SCN-based alloys to offer heterogeneous structure and thermally stable IMCs is markedly required to attain a prominent combination of viscoplastic creep with a high creep resistance in microelectronic alloy solders. The morphology of IMCs in Fig.(2b) for the SCN-0.1%Al solder was characterized by EDS analysis (Fig. 3). The block Cu_6Sn_5 and rod-like (Cu, Ni)$_6$ Sn_5 IMCs with a high thermal stability can be clearly established in the SCN-0.1%Al alloy. Compared with Cu_6Sn_5 and (Cu, Ni)$_6$ Sn_5 phases, fine Al_2Ni_3 and Al_2Cu particles cannot be detected clearly due to the use of 0.1%Al element to form of Al_2Ni_3 and Al_2Cu IMCs in SCN-0.1%Al alloy, which are established and resolved by XRD as shown in Fig.(1).

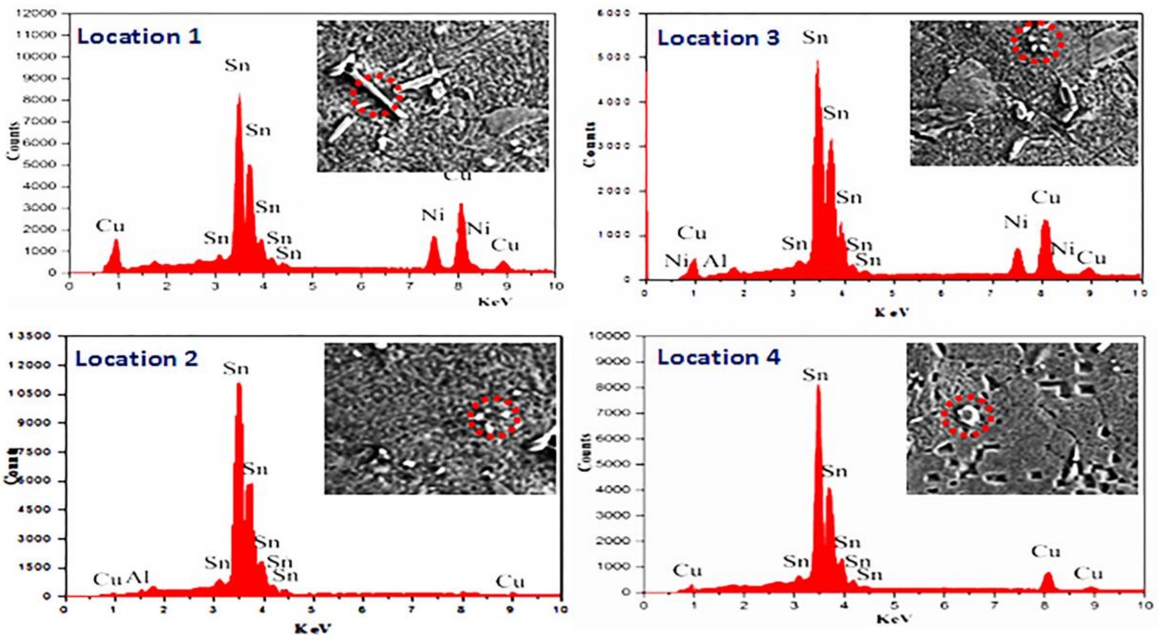

Fig. (3): EDS analysis of different phases in (SCN-0.1%Al) alloy sample

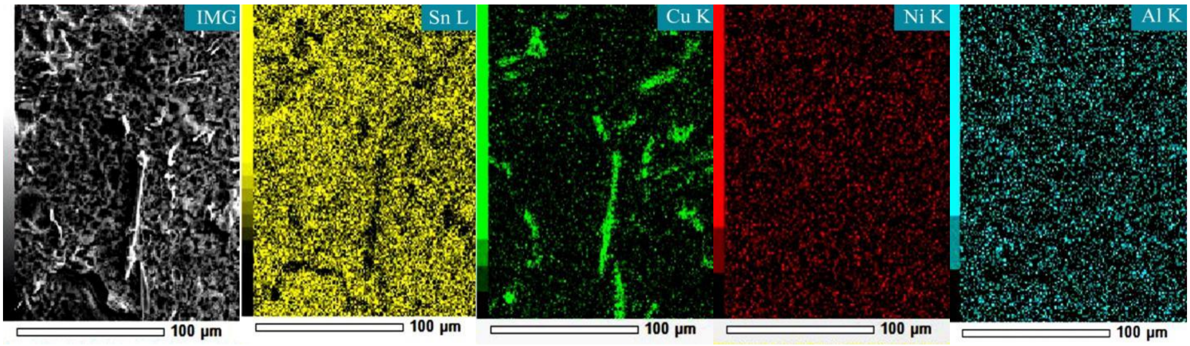

Fig. (4): The EPMA of (SCN-0.2Al) solder alloy

These fine precipitates however formed new nucleation sites which can hinder the dislocation motion in dislocation creep. The development of coarse IMCs in the SCN-*x*Al alloys leads to a higher ductility, and consequently the absence of micro-cracks, owing to the released stresses concentration at interface boundaries. The morphology of SCN-0.2%Al solder in Fig.(2c) was characterized by elemental mapping analysis EPMA of deep-etched alloy specimen (Fig. 4). The appealing effect of Al addition is comparable to that was established in previous studies [26-28]. This specifies that microalloying of Al to plain SCN solder could suppress the coarsening of β-Sn grains, control the growth rate of IMC particles in the bulk solder and construct a network-like structure, which successively modified the creep resistance and ductility of the newly developed solders.

Tensile property

Fig. (5a) depicts the room-temperature tensile stress-strain responses of precipitation-strengthened SCN, SCN-0.1wt.% Al and SCN-0.2 wt.%Al alloys tested at 5.3 x 10^{-4} s^{-1}. The mean values of the yield strength (YS), ultimate tensile strength (UTS), and elongation are compared with those previously reported of the SC alloy (Table 2). The YS and UTS of the SCN solder are slightly decreased respectively, from 37.2 and 39.2 MPa to 34.3 and 36.0 MPa and eventually to 31.5 and 34.3MPa with increasing Al content from 0.1 to 0.2wt.%. Meanwhile, the exceptional ductility increases from 55% to 69 % and 67%, respectively. Notably, the YS, UTS and ductility of SCN-0.1wt.% Al and SCN-0.2 wt.% Al alloys are significantly higher than those of the SC alloys, as seen in Table (2). Increasing the ductility can offer a new generation of enhanced strength-ductility trade-off (SDT) alloys with advancing elastic

Table (2): Tensile properties of SC, SCN, SCN-0.1Al and SCN-0.2Al solder alloys at T = 25 °C and $\dot{\varepsilon}$ = 5.3 x 10^{-4} s^{-1}

Alloy	UTS (MPa)	YS (MPa)	Elongation (%)	Young's modulus (GPa)
Sn-0.7Cu-0.2Ni	39.2	37.2	55	21.9
Sn-0.7Cu-0.2Ni-0.1Al	36.0	34.3	69	21.1
Sn-0.7Cu-0.2Ni-0.2Al	34.3	31.5	67	20.4
Sn-0.7Cu [22]	28.0	20.4	44	-----

compliance and plastic energy dissipation ability for mobile products industry.

Viscoplastic creep curves

As the two alloys SCN-0.1wt.% Al and SCN-0.2 wt.%Al show a satisfactory enhanced SDT after the heterogeneous structures were produced by cold-drawn and temperature-annealing, it was performed to tensile creep testing in order to confirm that a successful combination of desirable ductility and viscoplastic creep was attained. Fig. (6) shows the creep curves of three alloys at room temperature under 15.6 MPa. The creep curves are characterized by three creep stages, which involve primary and steady state creep as well as tertiary creep. Notably, the decelerating creep stage of SCN alloy becomes shorter after Al-microalloying. Although the creep stress is constant, the strains increase very fast in the Al-containing solders, especially in the SCN-0.2 wt.%Al alloy, since these alloys exhibit viscoplastic deformation caused by their heterogeneous structures.

The creep rate $\dot{\varepsilon}_m$ is one of the foremost imperative parameters of creep behavior in engineering assessments. Because the creep tests

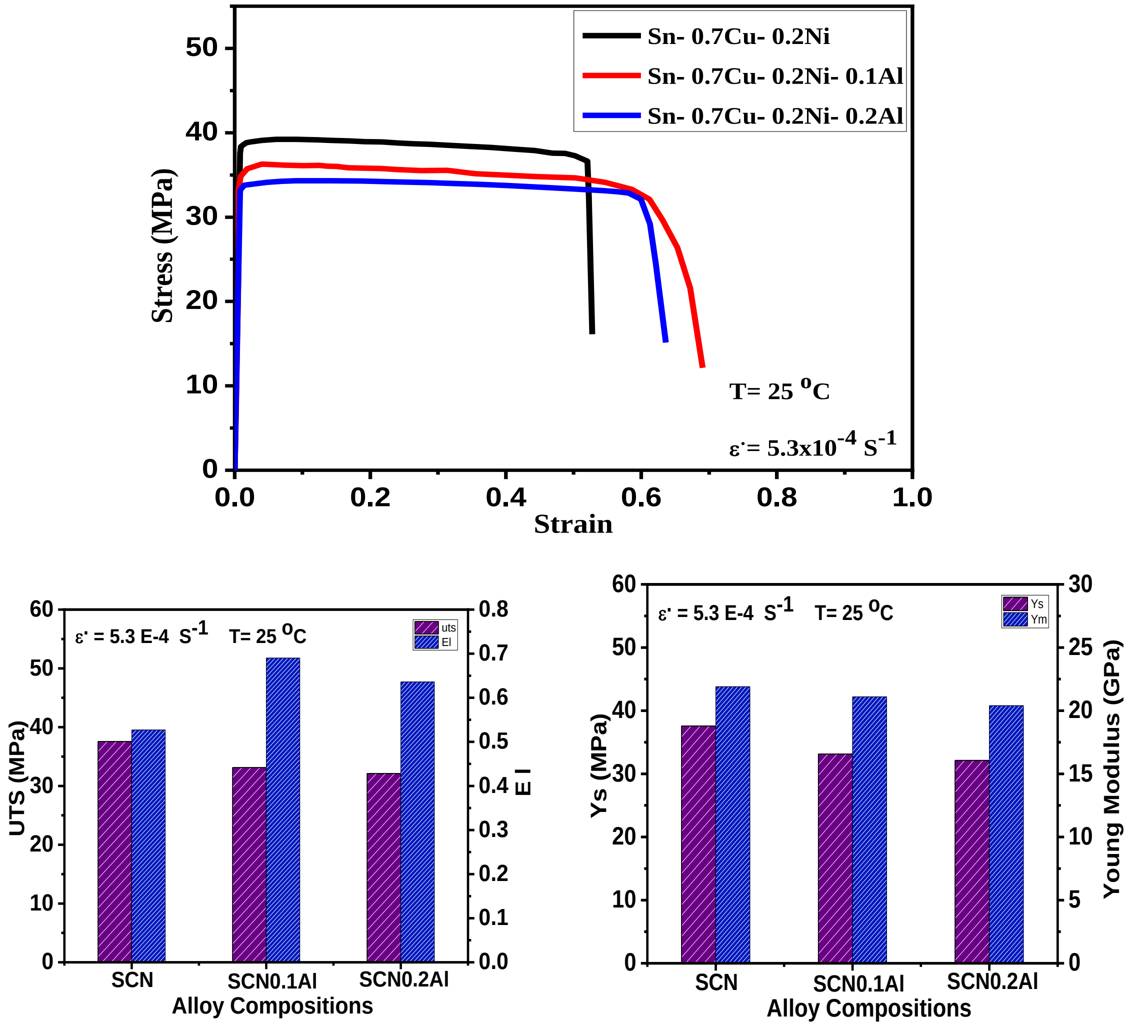

Fig. (5): Tensile stress-strain curves of (SCN), (SCN-0.1Al) and (SCN-0.2Al) alloys at T=25°C, $\dot{\varepsilon}$=5.3x10^{-4}s^{-1} and corresponding histograms comparing the ultimate tensile strength (UTS), yield strength (YS), ductility (El) and Young modulus (YM).

are performed at constant stress and temperatures, the change in the creep rate $\dot{\varepsilon}$ suggests that the internal stress has been altered during time. The $\dot{\varepsilon}_m$, which can be evaluated from the slope of creep curves as a function of strain, is presented in Fig.(6). Notably, the steady state creep stages of SCN, SCN-0.1wt.% Al and SCN-0.2 wt.%Al are characterized by a well-defined linear creep behavior with minimum creep rates, which are highlighted by circle markers. The minimum creep rates of 3.1 x 10^{-5} s^{-1}, 5.4 x 10^{-5} s^{-1}and 2.0 x 10^{-4} s^{-1}, respectively, are attained for three alloys. Both the minimum creep rates of the SCN and SCN-0.1wt.% Al alloys are characterized by less pronounced transient creep rate and realized after 0.22 and 0. 17% strain, respectively, while those of SCN-0.2wt.% Al alloy are attained at a larger strain of 0.24%. This means that the SCN-0.1wt.% Al alloy showed the minimum creep rate at less creep strain as compared to the other two alloys.

Diffusional creep appears to be more pertinent owing to sufficient level of loading. However, the secondary creep deformation process inhabits ~ 15-35% of the entire creep life time, where the deformation resistance is steady through this stage. Owing to the high homologous temperature, strain hardening and plastic deformation escorted the dynamic recovery that takes place during creep deformation process. Then, the deformation hardening and dynamic recovery are balanced at the equilibrium state, where the alloy solders could deform at constant rate, while the strain energy maintains at a definite level.

Interestingly, the most important result is the combination of appropriate creep resistance and large strain of 0.51% that can be achieved in SCN-0.1 wt.%Al solder compared with strain of 0.32%

and 0.45% for the SCN and SCN-0.2wt.% Al alloys, indicating that the deformation resistance is longstanding during that stage in the SCN-0.1 wt.%Al solder. Bulk compliance and plastic energy dissipation ability, in which the basic material properties could be adjusted for effective crack driving force toughening mechanisms, play a significant role in drop impact performance enrichment. It can be largely enhanced by creation of heterogeneous structure. Hence, the high creep resistance and large strain of 0.51% achieved in SCN-0.1 wt.%Al solder played a significant role in drop impact performance enrichment of the Pb-free SCN-0.1 wt.%Al solder interconnections in electronic devices. Similar trends are also found in low Ag-content SAC105 solders in recent studies **[**27, 28**]**. They suggested that Fe-bearing solders have shown to form large primary β-Sn grains. Besides, the formation of large $FeSn_2$ IMC particles caused a significant reduction in the elastic modulus and yield strength with increasing creep strain. Although the IMCs can strengthen the Sn matrix of solder, their influences are affected by their size and distribution inside solder matrix, which are considered the foremost factors affecting the viscoplastic creep.

Consistent with these results, the formation of thin and coarse dispersed IMC particles can extensively enhance the viscoplastic deformation resistance of the SCN-0.1wt.%Al solder. And also confine the microstructure progress inspired by dislocation movement. If the $(Cu,Ni)_6Sn_5$ IMCs are coarsen into large bars as seen in the SCN-0.2wt.%Al solder (Fig. 2), its strengthen effect will drop severely. Hence, it is easygoing to fracture. Cracking is expected to occur definitely at the large phase boundaries of $(Cu,Ni)_6Sn_5$ IMCs, since the deformation creep has occurred at higher strain rate, as seen in Fig. (6), wherein the minimum creep rate of the SCN-0.2wt.% Al solder was attained at a higher strain rate of 2.0 x 10^{-4} s^{-1} as compared to the other two alloys. Therefore, decreasing the actual crack driving force by crack tip across different energy dissipation processes leads to enhancing the extrinsic toughening mechanism.

Viscoplastic creep mechanisms of solders

From tensile creep tests, the influence of testing temperatures and applied stresses on creep characteristics are attained for the three alloys. A few representative creep curves for the SCN-0.1wt.% Al alloy sample are presented in Fig. (7). It is seen that the creep strain and creep rate are significantly increased with increasing both the stress and temperature. This could ascribe to the creation of new dislocation sources through the initial stage of creep. Since the applied stress could develop the driving force for increasing the density and mobility of dislocations, the creep rates are improved. Although the creep strain and creep rate are controlled by stress at room temperature, its effect could increase at high temperatures. The aforementioned effect of such increase in strain response could be prompted by their heterogeneous structure, where the Al-containing solders display viscoplastic deformations more willingly than common creep. Owing to the larger number of fine dispersed Cu_6Sn_5 and $(Cu,Ni)_6Sn_5$ IMC precipitates in the SCN solder, the pinning effects for dislocations are increased in plain solder compared to those of the Al-containing solders.

The minimum creep rate (steady state) $\dot{\varepsilon}_m$ is one of the significant creep parameters for structural and manufacturing studies. Its stress σ and temperature *T* dependence are often expressed by the following hyperbolic sine equation [19]:

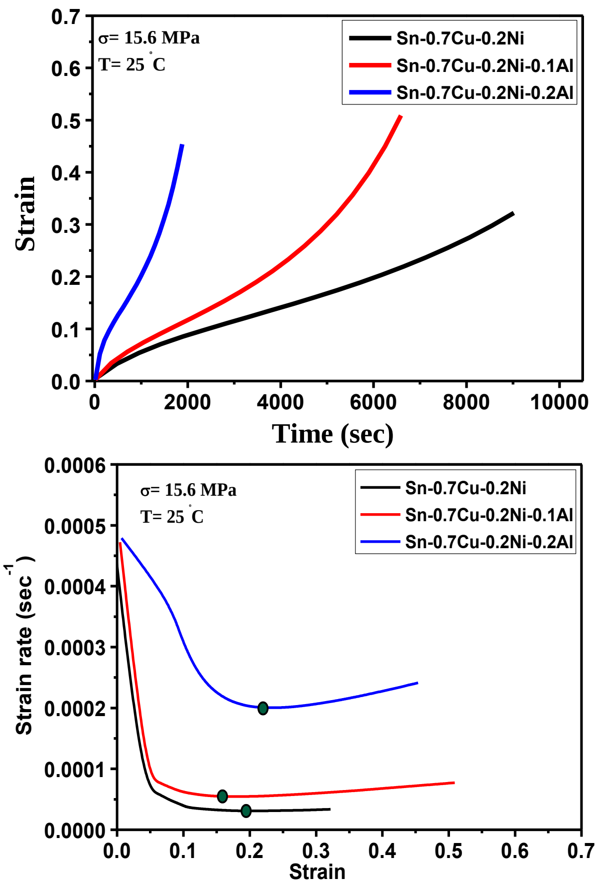

Fig. (6): Comparison of creep curves and creep rate–strain curves at T = 25 C° and *σ* = 15.6 MPa of (SCN), (SCN-0.1Al) and (SCN-0.2Al) alloys

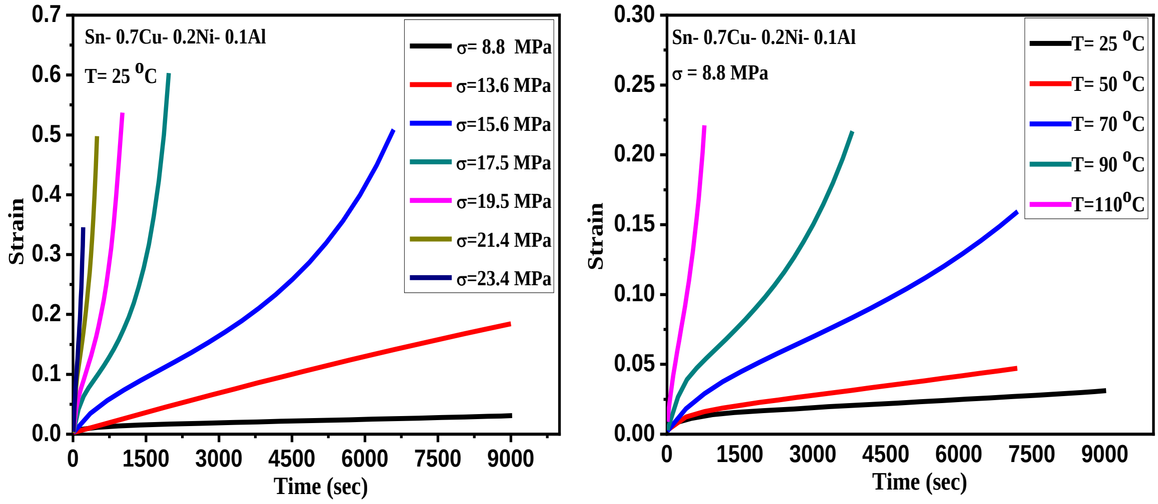

Fig. (7): Variation of creep strain-time of SCN-0.1%Al with applied stresses at constant temperature of 25 °C and with different temperatures at constant stress of 8.8 MPa. (Similar curves were obtained for (SCN) and (SCN-0.2%Al) alloys not shown here.).

$$\dot{\varepsilon}_m = A\,\{\sinh(\alpha\sigma)\}^n \exp(-Q/RT) \qquad (1)$$

Where A (s^{-1}) and α (MPa^{-1}) are the material constants, $\alpha = \beta/n_1$ is the stress level parameter, n is the stress exponent, R is the gas constant and Q (kJ/mol) is the creep activation energy. The appealing of hyperbolic sine analysis is their precisely incorporate both low- and high stress data in a single model reflecting power-law and power law breakdown behavior, respectively. For the low stress level (power law) and high stress level (exponential law), respectively, Eq. (1) can be expressed as [29]:

$$\dot{\varepsilon}_m = A_1\,(\sigma)^{n_1} \qquad (2)$$

$$\dot{\varepsilon}_m = A_2\,(\sigma)^{\beta} \qquad (3)$$

The constants β and n_1 are assessed from equations (2) and (3) and the values of parameter α are listed in Table (3). Then, the values of n and Q can be attained from the following equations:

$$n = \left.\frac{\partial ln\varepsilon_m}{\partial \ln\{\sinh(\alpha\sigma)\}}\right|_T \qquad (4)$$

$$Q = \left.\frac{\partial ln\varepsilon_m}{\partial \ln(1/T)}\right|_\sigma \qquad (5)$$

Fig. (8) shows the relationship between ln $\dot{\varepsilon}_m$ and $\ln\{\sinh(\alpha\sigma)\}$ and Fig. (9) reveals the relation between ln $\dot{\varepsilon}_m$ and $1/T$ of three alloys, respectively. The values of n and Q are listed in Table (3). The n value was estimated to be in the range of 4.4-5.7 for the three alloys, notifying equivalent characteristics as those of the SAC(157) and Sn-6.5Zn-based alloys, which display n values of 3.9-4.7and 4.1-5.0, respectively [30, 31]. The small variation of n values recommends the microstructure stability and sensitivity of the Sn–0.7Cu-0.2Ni to Al-microalloying at high processing temperatures.

Table (3): Activation energy (Q), stress exponent (n) and (α) values for Sn-0.7Cu-0.2Ni, Sn-0.7Cu-0.2Ni-0.1Al and Sn-0.7Cu-0.2Ni-0.2Alsolder alloys

Alloy	Q (kJ/mol)	Temperature (°C)	α	n
Sn-0.7Cu-0.2Ni	53.89	25	0.055	5.7
		70	0.098	5.0
		110	0.130	4.9
Sn-0.7Cu-0.2Ni-0.1Al	51.58	25	0.055	5.3
		70	0.098	4.7
		110	0.130	4.6
Sn-0.7Cu-0.2Ni-0.2Al	46.76	25	0.055	5.1
		70	0.098	4.6
		110	0.130	4.4

As the n values of both Al-containing alloys and plain SCN are in the same order, the same creep mechanism is active in all alloys, as was found in precipitation strengthened alloys on account of the formation of IMCs in the present alloys. This specifies that creep mechanism is the dislocation climb regime controlled the Sn–0.7Cu-0.2Ni–xAl alloy series. Notably, precipitation strengthening effect is predominant at room temperature since the n value decreases slightly with increasing the temperature.

Furthermore, the effect of the temperature on the creep rate is illustrated in Fig. (9), where the Q value of SCN is slightly decreased from 53.89 to 46.76 KJ/mol in the Al-containing SCN alloys.

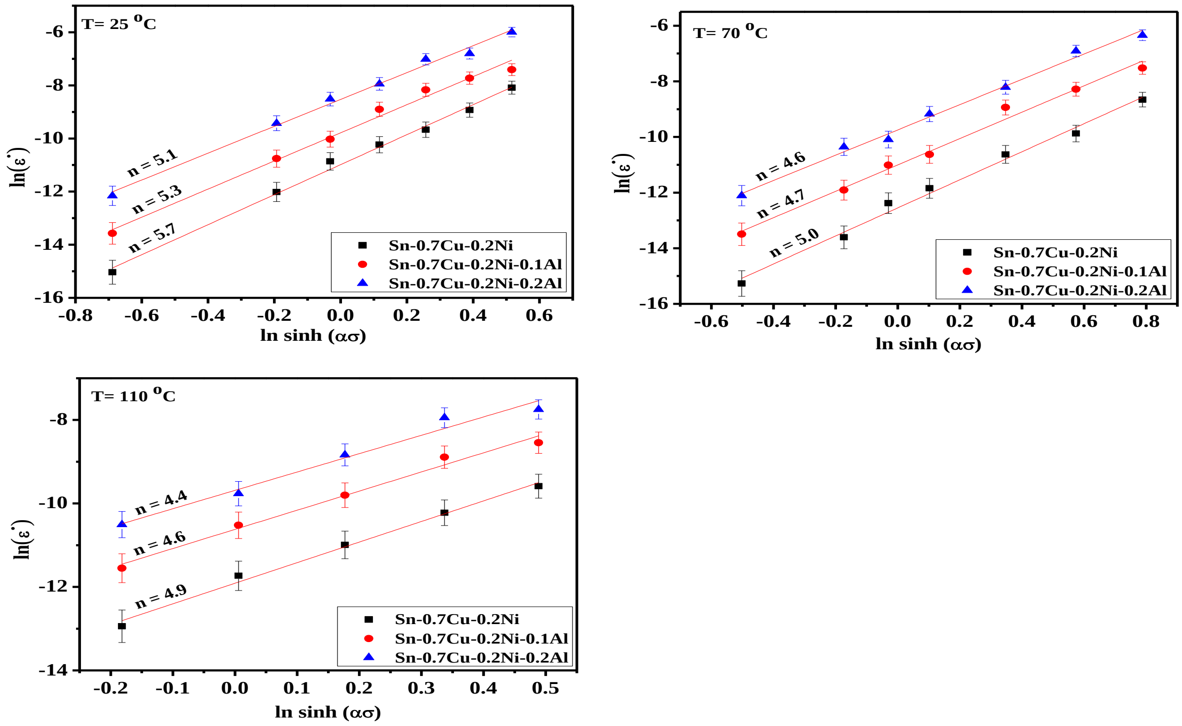

Fig. (8): Relationship between ln[sinh(as)] and ln($\dot{\varepsilon}$) for determination the stress exponent values at T = 25, T = 70 and T = 110 °C of (SCN), (SCN-0.1Al) and (SCN-0.2Al) alloys

Furthermore, the effect of the temperature on the creep rate is illustrated in Fig. (9), where the *Q* value of SCN is slightly decreased from 53.89 to 46.76 KJ/mol in the Al-containing SCN alloys. These *Q* values are close to those associated with the dislocation pipe diffusion of the Sn-based alloys [30, 32]. It is known that the activated processes that proceed in pure metals cannot arise in the precipitation-strengthened alloys [33].

In the present study, the precipitations of fine Cu_6Sn_5 and $(Cu, Ni)_6$ Sn_5 phases in the SCN alloy are in a semi-coherent link with the alloy matrix. In contrast, the large bars of $(Cu, Ni)_6Sn_5$ IMCs formed in the Al-containing SCN alloys are incoherent with β-Sn matrix, where the dislocations may be annihilated at incoherent interface boundaries. In other words, the interface boundaries of $(Cu, Ni)_6Sn_5$ IMCs particles may be considered a sources of vacancies required for diffusion mechanisms, which assists the dislocations climb when they come across the IMC particles. Owing to the higher hardness of IMC particles compared to that of the β-Sn matrix, the particle cutting mechanism appears to be incredible in these solders. Hence, the dislocation climb overhead the IMC particle seems to be satisfactory, since the *Q* value is generally coupled with the binding energy among the dislocations and IMC particles. The high dislocation density caused by IMC particles proposes that dislocation pipe diffusion may supply a short circuit for diffusion. It can allow the prompt motion of dislocation climb to passage at high creep strain rates. Although the present results clarify that the Sn–0.7Cu-0.2Ni–xAl alloy series exhibit an approximately comparable creep rate to that of pure Sn, the present alloys could operate at higher applied stresses than pure metals.

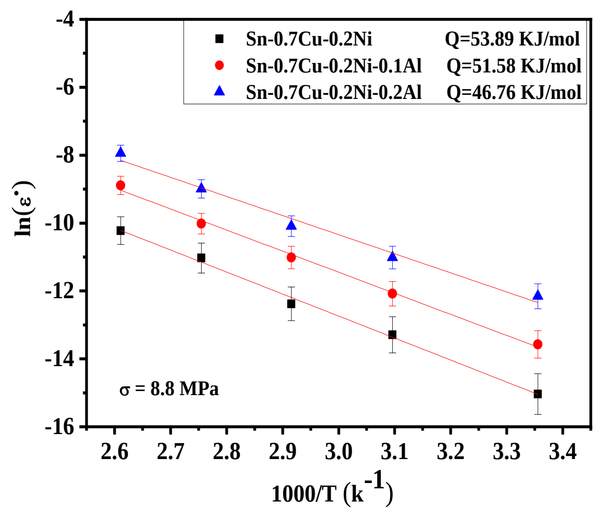

Fig. (9): Temperature dependence of steady state creep rate for (SCN), (SCN-0.1Al) and (SCN-0.2Al) alloys

Conclusions

The strength, ductility and creep behavior of a newly developed Sn–0.7Cu-0.2Ni (wt.%) alloy have been investigated. The effect of Al-microalloying on the high temperature creep properties have been analyzed. The following conclusions can be drawn.

1) The microstructural characterization of the Sn–0.7Cu-0.2Ni alloy exhibited the formation of fine and more stable $(Cu,Ni)_6Sn_5$ IMC particles that inhibit the polymorphic phase transition of Cu_6Sn_5 IMC particles owing to Ni content.

2) After Al-microalloying, the morphology of IMCs is dependent on the aluminum content although the Sn–0.7Cu-0.2Ni–xAl alloys exhibit heterogeneous structure with an additional fine Al_3Ni_2 and Al_2Cu IMC phases and coarse $(Cu,Ni)_6Sn_5$ IMCs.

3) The SCN-0.1 wt.%Al solder alloy displays a unique combination of enhanced creep resistance and large strain of 0.51% although the SCN and SCN-0.2wt.%Al alloys showed either reasonable creep resistance or outstanding ductility behavior of 0.45%, respectively .

4) The minimum creep rate of SCN-0.1 wt.%Al is only slightly higher than that of SCN. This may be ascribable to the minimal strengthening effect of $(Cu,Ni)_6Sn_5$ phase as its size becomes slightly large.

5) In the SCN-0.1 wt.%Al alloy, the formation of fine Al_3Ni_2 and Al_2Cu IMC phases and coarse $(Cu,Ni)_6Sn_5$ IMCs leads to a slight reduction in UTS, elastic modulus and 0.2%YS, but a large increase in the ductility up to ~69% is attained. As a result, Al-microalloying can further enhances the bulk conformity and plastic energy debauchery ability of the solder, which plays an imperative role in drop impact performance enhancement of the innovative interconnecting applications.

6) The *n* values of 4.4 to 5.7 coupled with the *Q* values of 46.67-53.89 kJ/mol recommended that the effective creep mechanism is dislocation climb controlled by pipe diffusion for the three alloys.

References

1. Salleh, M. M., McDonald, S. D., and Nogita, K. (2017) Effects of Ni and TiO_2 Additions in as-reflowed and Annealed Sn0. 7Cu Solders on Cu Substrates, *Journal of Materials Processing Technology*, **242**, 235-245.
2. Ramli, M. I. I., Salleh, M. M., Yasuda, H., Chaiprapa, J. and Nogita, K. (2020) The Effect of Bi on the Microstructure, Electrical, Wettability and Mechanical Properties of Sn-0.7 Cu-0.05 Ni Alloys for High Strength Soldering, *Materials & Design*, **186**, 108281.
3. Zeng, G., McDonald, S. D., Gu, Q., Terada, Y., Uesugi, K., Yasuda, H. and Nogita, K. (2015) The Influence of Ni and Zn Additions on Microstructure and Phase Transformations in Sn–0.7 Cu/Cu Solder Joints, *Acta Materialia*, **83**, 357-371.
4. Wang, Y., Wang, G., Song, K. and Zhang, K. (2017) Effect of Ni Addition on the Wettability and Microstructure of Sn2. 5Ag0. 7Cu0. 1RE Solder Alloy, *Materials & Design*, **119**, 219-224.
5. Ventura, T., Terzi, S., Rappaz, M. and Dahle, A. K. (2011) Effects of Ni Additions, Trace Elements and Solidification Kinetics on Microstructure Formation in Sn–0.7 Cu Solder, *Acta Materialia*, **59**(10), 4197-4206.
6. Zeng, G., McDonald, S. D., Read, J. J., Gu, Q. and Nogita, K. (2014) Kinetics of The Polymorphic Phase Transformation of Cu6Sn5, *Acta materialia*, **69**, 135-148.
7. Rizvi, M. J., Bailey, C., Chan, Y. C., Islam, M. N. and Lu, H. (2007), Effect of Adding 0.3 wt% Ni into the Sn–0.7 wt% Cu Solder, Part II. Growth of Intermetallic Layer with Cu During Wetting and Aging, *Journal of alloys and compounds*, **438**(1-2), 122-128.
8. Laurila, T., Hurtig, J., Vuorinen, V. and Kivilahti, J. K. (2009) Effect of Ag, Fe, Au and Ni on the Growth Kinetics of Sn–Cu Intermetallic Compound Layers, *Microelectronics Reliability*, **49**(3), 242-247.
9. Nogita, K. (2010) Stabilisation of Cu6Sn5 by Ni in Sn-0.7 Cu-0.05 Ni Lead-Free Solder Alloys, *Intermetallics*, **18**(1), 145-149.
10. Wang, J. X., Xue, S. B., Han, Z. J., Yu, S. L., Chen, Y., Shi, Y. P. and Wang, H. (2009) Effects of Rare Earth Ce on Microstructures, Solderability of Sn–Ag–Cu and Sn–Cu–Ni Solders as well as Mechanical Properties of Soldered Joints, *Journal of Alloys and Compounds*, **467**(1-2), 219-226.
11. Yu, C. Y. and Duh, J. G. (2011) Stabilization of Hexagonal Cu6 (Sn, Zn) 5 by Minor Zn Doping of Sn-Based Solder Joints, *Scripta Materialia*, **65**(9), 783-786.

12. Zeng, G., McDonald, S. D., Gu, Q., Suenaga, S., Zhang, Y., Chen, J. and Nogita, K. (2013) Phase Stability and Thermal Expansion Behavior of Cu6Sn5 Intermetallics Doped with Zn, Au and In, *Intermetallics*, **43**, 85-98.
13. Shnawah, D. A., Said, S. B. M., Sabri, M. F. M., Badruddin, I. A., and Che, F. X. (2012). High-Reliability Low-Ag-Content Sn-Ag-Cu Solder Joints for electronics Applications, *Journal of electronic materials*, **41**(9), 2631-2658.
14. Wang, J. X., Xue, S. B., Han, Z. J., Yu, S. L., Chen, Y., Shi, Y. P. and Wang, H. (2009) Effects of Rare Earth Ce on Microstructures, Solderability of Sn–Ag–Cu and Sn–Cu–Ni Solders as well as Mechanical Properties of Soldered Joints, *Journal of Alloys and Compounds*, **467**(1-2), 219-226.
15. Nogita, K. (2010) Stabilisation of Cu6Sn5 by Ni in Sn-0.7 Cu-0.05 Ni Lead-Free Solder Alloys, *Intermetallics*, **18**(1), 145-149.
16. Zeng, G., Xue, S., Gao, L., Zhang, L., Hu, Y. and Lai, Z. (2011) Interfacial Microstructure and Properties of Sn–0.7 Cu–0.05 Ni/Cu Solder Joint with Rare Earth Nd Addition, *Journal of Alloys and Compounds*, **509**(25), 7152-7161.
17. Liu, S., Xue, S. B., Xue, P. and Luo, D. X. (2015) Present Status of Sn–Zn Lead-Free Solders Bearing Alloying Elements, *Journal of Materials Science: Materials in Electronics*, **26**(7), 4389-4411.
18. Lai, Z. and Ye, D. (2016) Effect of Al on the Microstructure and Properties of Sn–0.7 Cu solder Alloy, *Journal of Materials Science: Materials in Electronics*, **27**(2), 1177-1183.
19. El-Daly, A. A., Ibrahiem, A. A., Abdo, M. A. and Eid, N. A. M. (2019) Viscoplastic Characterization and Mechanical Strength of novel Sn–1.7 Ag–0.7 Cu Lead-Free Solder Alloys with Microalloying of Te and Co, *Journal of Materials Science: Materials in Electronics*, **30**(14), 12937-12949.
20. Saad, G., Fayek, S. A., Fawzy, A., Soliman, H. N. and Mohammed, G. (2010) Deformation Characteristics of Al-4043 Alloy, *Materials Science and Engineering: A*, **527**(4-5), 904-910.
21. El−Daly1, A., Eladly, S. A., Mohamed, A., Elmosalami, T. A. and Dawood, M. S. (2020) Improvement of Strength-Ductility Trade-off in a Sn–0.7Cu–0.2Ni Lead-Free Solder Alloys through Al-Microalloying, *J.Mater. Sci.: Mater. Electron*., **13**, 8649-8661.
22. Ramli, M. I. I., Salleh, M. M., Yasuda, H., Chaiprapa, J. and Nogita, K. (2020) The Effect of Bi on the Microstructure, Electrical, Wettability and Mechanical Properties of Sn-0.7 Cu-0.05 Ni Alloys for High Strength Soldering, *Materials & Design*, 1**86**, 108281.
23. El-Daly, A. A. and Hammad, A. E. (2011) Development of High Strength Sn–0.7 Cu Solders with the Addition of Small Amount of Ag and In, *Journal of Alloys and Compounds*, **509**(34), 8554-8560.
24. Wu, S. W., Wang, G., Wang, Q., Jia, Y. D., Yi, J., Zhai, Q. J., ... and Liaw, P. K. (2019) Enhancement of Strength-Ductility Trade-off in a High-Entropy Alloy through a Heterogeneous Structure, *Acta Materialia*, **165**, 444-458.
25. Croteau, J. R., Griffiths, S., Rossell, M. D., Leinenbach, C., Kenel, C., Jansen, V., ... and Vo, N. Q. (2018) Microstructure and Mechanical Properties of Al-Mg-Zr Alloys Processed By Selective Laser Melting, *Acta Materialia*, **153**, 35-44.
26. El-Daly, A. A., El-Taher, A. M., and Dalloul, T. R. (2014) Improved Creep Resistance and Thermal Behavior of Ni-Doped Sn–3.0 Ag–0.5 Cu Lead-Free Solder, *Journal of alloys and compounds*, **587**, 32-39.
27. Shnawah, D. A. A., Said, S. B. M., Sabri, M. F. M., Badruddin, I. A. and Che, F. X. (2012) Microstructure, Mechanical, and Thermal Properties of the Sn–1Ag–0.5 Cu Solder Alloy Bearing Fe for Electronics Applications, *Materials Science and Engineering: A*, **551**, 160-168.
28. Shnawah, D. A. A., Said, S. B. M., Sabri, M. F. M., Badruddin, I. A., and Che, F. X. (2012) Novel Fe-Containing Sn–1Ag–0.5 Cu Lead-Free Solder Alloy with Further Enhanced Elastic Compliance and Plastic Energy Dissipation Ability for Mobile Products, *Microelectronics Reliability*, **52**(11), 2701-2708.
29. Senthilkumar, V., Balaji, A. and Narayanasamy, R. (2012) Analysis of Hot Deformation Behavior of Al 5083–TiC Nanocomposite Using Constitutive and Dynamic Material Models, *Materials & Design*, **37**, 102-110.
30. El-Daly, A. A., El-Taher, A. M. and Gouda, S. (2015) Development of New Multicomponent

Sn–Ag–Cu–Bi lead-Free Solders for Low-Cost Commercial Electronic Assembly, *Journal of Alloys and Compounds*, **627**, 268-275.

31. El-Daly, A. A., Desoky, W. M., Saad, A. F., Mansor, N. A., Lotfy, E. H., Abd-Elmoniem, H. M. and Hashem, H. (2015) The Effect of Undercooling on the Microstructure and Tensile Properties of Hypoeutectic Sn–6.5 Zn–xCu Pb-Free Solders, *Materials & Design*, **80**, 152-162.
El-Daly, A. A., Al-Ganainy, G. S., Fawzy, A. and Younis, M. J. (2014) Structural Characterization and Creep Resistance of Nano-Silicon Carbide Reinforced Sn–1.0 Ag–0.5 Cu Lead-Free Solder Alloy, *Materials & Design*, **55**, 837-845.
32. Wu, C. L. and Huang, M. L. (2002) Creep Behavior of Eutectic Sn-Cu Lead-Free Solder Alloy, *Journal of electronic materials*, **31**(5), 442-448.